Comparison of acoustic retroreflection from corner cube arrays using FDTD simulation

Hugo Caldwell (1), Densil Cabrera (1)

(1) School of Architecture, Design and Planning, The University of Sydney, Sydney, Australia

ABSTRACT

Acoustically retroreflective surfaces reflect sound back to the source, over a wide range of possible source positions. This paper explores their potential use in architecture, in the form of an extensive array of square trihedral corner cubes which could be used for reducing speech distraction in multi-talker environments. The retroreflective effectiveness of a corner cube array surface is investigated by simulation using the finite-difference time-domain (FDTD) method. The factors investigated were the distance of an omnidirectional source to the array surface (1, 2 and 3 m) and the size of the individual corner cubes that make up the array surface (0.3, 0.6, 0.9 and 1.2 m edge lengths), in the 250 Hz – 8 kHz octave bands. Retroreflection performance was assessed by (i) the energy reflected by the array surface back to the source position, and (ii) the spatial decay rate of reflected energy as a function of distance from source. Results indicate that a retroreflective array surface comprising corner cubes with edge lengths of 0.3 m and 0.6 m have most potential as surface treatments in architectural applications over the range of distances simulated.

1 INTRODUCTION

As opposed to specular reflections or scattering, the concept of retroreflection is that a surface reflects energy back to the source over a wide range of possible source positions. The simplest approach to creating retroreflection is three mirrored surfaces joined by a concave right angle – known as a corner cube, which is commonly used in radar and optics. For applications in optics, a retroreflective element can be very small, due to the small wavelengths of visible light and some examples include high visibility clothing and road signs. Optical corner cubes are commonly used for surveying instruments, and as arrays in photoelectric sensor reflectors and bicycle reflectors. As radar uses longer wavelengths, the corner cube size must be correspondingly larger.

The intentional use of retroreflectors in architectural acoustics, as arrays, is very unusual. The size of an acoustic retroreflector would have to be substantially larger than optical retroreflectors, in order to reflect sound waves back to the source, as sound wavelengths are much larger than optical wavelengths. The size requirement of single acoustic retroreflectors is one reason why retroreflection is scarcely used in architectural design. An array of many acoustic retroreflectors produces focusing back to the source, although the focusing may be incoherent due to the variety of path lengths involved. A simple acoustic retroreflector which could be arrayed has the same form corner cubes found in optics and radar: three reflective surfaces joined by a concave right angle (Figure 1.A).

There are some instances of building facades that contain acoustically retroreflective elements, although not intended for that purpose. Crawford (1991) noted that certain building facades at the University of California Berkeley campus may support acoustic retroreflection. He discussed that handclaps in the vicinity of a façade comprising an array of corner cubes yielded stronger audible reflections than when the corner cubes were not in view. Cox and D'Antonio (2009) also elaborate on the concept of retroreflection in two dimensions, where two perpendicular surfaces, which might be part of a 'saw-tooth' configuration, will provide a focused second order reflection back towards the source, a concept sometimes used to provide acoustic support on auditorium stages.

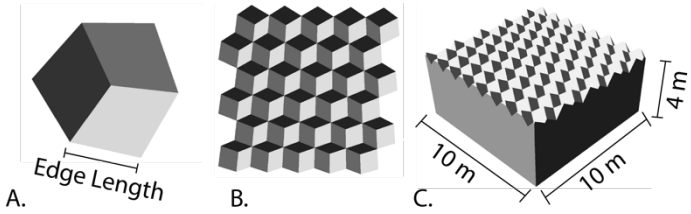

Figure 1: Visualisation of modelled retroreflectors: A. Single square trihedral corner cube with indicative edge length; B. Array of 30 corner cubes; C. Array of corner cubes as a ceiling of a room (anechoic walls and floor were used in the simulations performed in this study)

In more complex cases, retroreflection could act on sound from multiple sources within the effective region of a retroreflective surface, thereby reflecting the sound of each source independently back to the respective source. This effect of retroreflection could have application in multi-talker environments, to help reduce distracting speech sounds through the theory of a reversed Lombard (Lombard, 1911) effect or Lombard reflex (Lau, 2008). A recent pilot study (Hannouch et al., 2018) has considered how this could be deployed as an open-plan office ceiling treatment. The present study will provide a basis for future consideration into the use of retroreflective surfaces in multi-talker environments to help with speech-related issues.

The potential of acoustic corner cube arrays has also been explored by Cabrera et al. (2018) in a case study of an unusual building façade in Shanghai that has an array of 255 corner cube reflectors (0.3 m edge lengths) overhanging the main entrance. Although the façade is outdoors and next to a busy road intersection, it was noticed that a clear retroreflection occurred with only one's own speech sounds or handclaps. Analysis of measured and simulated (finite-difference time-domain) reflections from the façade indicate strong retroreflection, providing substantial support for one's own voice in the high frequency range (especially in the 4 kHz and 8 kHz octave bands), while still providing a small noticeable retroreflection at lower frequencies (2 kHz, and weakly at 1 kHz at distances close to the facade).

All of the above studies present cases where retroreflection is limited to either surface or element size, or number of retroreflective elements. This presents an area of retroreflection that has not yet been explored systematically in architectural acoustics. How big should retroreflective elements be in an architectural surface, in order to return maximum sound to the source, and to reflect minimum sound elsewhere? The answer to this question may depend on the distance between the source and the surface, and will be frequency-dependent. Hypothetically, there is a trade-off between low-frequency performance (larger corner cubes support lower frequency retroreflection) and the overall degree of retroreflectivity (smaller corner cubes provide more individual retroreflective elements). This is examined through computational simulations using finite-difference time-domain (FDTD) method.

1.1 Finite-Difference Time-Domain Method (FDTD)

Acoustic modelling methods are usually separated in two separate fields: geometry-based and wave-based methods. While geometric methods model sound ray paths, wave based methods use a numerical solution to solve the wave equation. For corner cube arrays of the scale investigated in this paper, complicated diffraction and scattering phenomena are expected to be important, especially at longer wavelengths, and such phenomena are not well-represented using ray techniques. In theory, a wave-based solution is preferable to determine the acoustic characteristics of a computational geometry, as a numerical method will better describe the sound field (Haapaniemi, 2012), (Saarelma, 2013), (Kowalczyk, 2009). However, the usability of such methods can have a high computational demand. FDTD is a very simple and well-known wave-based method.

The FDTD method is based on a wave-based propagation model in an isotropic environment in one or more dimensions, first presented by Yee (1966). Although mostly applied to electromagnetic theory to begin with, the concept of this wave-based model has been adapted to acoustic simulations. A mesh structure that forms a geometry is used for wave propagation calculations, where nodes (or "Yee cells") are placed in a regular spatial grid where the sampling frequency of the simulation dictates the size of each node. The FDTD scheme will then update

the spatial grid (Yee grid) node by node as the wave simulation progresses. This method is preferable for computational modelling as very small nodes will reduce error in discretising the wave equation. A first approach was proposed by Smith (1992), Smith and Van Duyne (1993) with regard to using digital waveguides for physical modelling, also known as digital waveguide meshes (DWM); mostly applied to musical acoustics. Both FDTD and DWM methods are similar in terms of wave propagation, but differ in processing applications.

Kowalczyk and Van Walstijn (2011) have been instrumental in developing a family of 3D compact explicit schemes, mostly based on a non-staggered rectilinear grid. Their approach has identified isotropic models that have been shown to be more accurate than the above 3D interpolated digital waveguide mesh methods. The standard rectilinear scheme (SRL) is the updated equivalent to the digital waveguide mesh (DWM) (Van Duyne, Smith, 1995) and has been defined as the standard leapfrog scheme (Bilbao, 2013), (Kowalczyk, Van Walstijn, 2011). It has since been widely implemented to solve room acoustic simulations, where more complex geometries can be examined, over unstructured grids, to adapt for irregular boundaries or geometrical elements. The common issue that arises within the FDTD implementation process is the computational cost (memory requirements are at an extreme), therefore this study utilised the Artemis High Performance Computing cluster. This service is provided to researchers for memory-intensive simulations, and is currently the most powerful research supercomputing infrastructure in the southern hemisphere.

2 METHOD

2.1 Geometry modelling

A computational room was built using Rhino 3D © with the dimensions (L:10 m, W:10 m, H:4 m) (Figure 1.C). Retroreflective corner cube arrays with corner cube edge lengths of 0.3 m, 0.6 m, 0.9 m and 1.2 m were modelled as a ceiling in four separate rooms. Also, a room with a flat reflective ceiling was modelled for comparison. To satisfy the requirements of the geometry importer for the FDTD solver, the geometries were converted to a mesh structure and triangulated using the *'Triangulatemesh'* command. Essentially, this command separates the geometric structure into triangular meshes, which are then converted to singular three-dimensional coordinates for each triangular mesh. The geometries were then exported as *'.obj'* files.

2.2 FDTD Implementation

The implementation of the FDTD solver used in this study was performed in several steps. ParallelFDTD (MIT Licensed, Saarelma, 2013) is an FDTD solver that utilizes the Computer Unified Device Architecture (CUDA) platform. This allows the solver to take advantage of parallel GPU-accelerated computing.
For the purpose of a trial, the solver was compiled on a Dell Precision 2250 machine, with a NVIDIA Quadro M1200 GPU which provided about 3.5 Gb of video memory with a compute capability of 5.0. This machine was used to test if geometries had been imported onto the solver successfully and for visualization purposes.

When these checks were successfully achieved, the ParallelFDTD solver was compiled on the Artemis High Performance Computing cluster. This service operates 108 NVIDIA V100 SXM2 GPU's, with 36 cores available per GPU node. Each GPU provides 16 GB of GPU RAM with a compute capability of 7.0 and can provide up to 7.8 teraFLOPS of GPU performance in double precision. The solver is then accessible through a Linux remote operator, with adequate storage capabilities. For the simulations, 4 nodes were requested (each 'job' is limited to 4 nodes) with a total of about 64 GB of RAM and 30 minutes of wall time on the GPU's.

The solver used the SRL 'leapfrog' scheme, with a known dispersion error and must therefore run at ten times the required sampling frequency to force an approximate 2% dispersion error. For this study, due to the extensive simulation parameters, the highest sampling frequency achieved was 90 kHz. This shows that even the most advanced GPU's available are still limited heavily by the requirements of such a solver. The geometric nodes are also determined by the sampling frequency, where the node size was ~ 0.006 m, resulting in over 1.5 billion nodes in the above geometry. The simulation contained two separate material coefficients, one for the room outer walls and floor and one for the retroreflective ceiling. Only the ceiling was made to be maximally reflective, while the room was maximally absorptive. Due to the limitations of the solver, the coefficients provided did not provide perfect absorptive or reflective boundaries. Efforts were made to optimise this and it was deemed sufficient for the purpose of this study. The simulation allowed for 10,000 time steps, which provided about 100 ms of output

signal (to fully capture the ceiling reflection in all cases). The source signal used was an anti-aliased delta function and was defined to be a transparent source (Schneider et al., 1998).

A horizontal plane of receivers was set in a grid covering the full length and width of the room, separated by 0.10 m (9801 receivers). To consider the effect of ceiling height, the plane of receivers was tested at three different heights, at 1, 2 and 3 m away from the ceiling. The source was placed at the centre of the room at the same heights as the receivers for each plane.

3 ANALYSIS

The output of the FDTD solver is in the form of individual impulse responses for each receiver, sampled at 48 kHz. For all simulations, the distance from the source to each receiver was used to determine when the direct sound would start. In order to separate the direct sound from the reflections, the simulation was also run with all surfaces absorptive, to allow subtraction of the direct sound. This subtraction was done over a window spanning the individual start and end points of the direct sound for each receiver impulse response. The reflected part of the impulse response was then filtered into octave bands, squared and summed to provide the reflected energy level, $L_{\mathrm{E,reflect}}$, for each receiver (equation 1). The results are expressed relative to the direct sound energy at 1 m from the source.

$$L_{\mathrm{E,reflect}} = 10\log\left[\sum_{n=N1}^{\mathrm{end}} x_{\mathrm{r}}^2(n) \Big/ \sum_{n=0}^{\mathrm{end}} x_{\mathrm{a,1m}}^2(n)\right] \quad (1)$$

Here, *n* is the sample number (time index) of a waveform for an individual receiver position, N1 and 'end' provide the first sample of data for the windowed reflecting sound to the last (i.e. end), x_{r} is the waveform of a receiver with a reflective ceiling and $x_{\mathrm{a,1m}}$ is the waveform of a receiver in an anechoic room at 1 m from the source.
The receiver plane was separated into 3 fields of interest, a small focal region with a radius of 0.15 m from the source, a near field (all receivers within 0.15 m to 1 m from the source) and a far field (all receivers from 1 m to 4.5 m from the source). The small focal region combined the energy from 8 receivers around the source within the 0.15 m radius, omitting the centre receiver (which sometimes yielded outlying values due to colocation with the source nodes). The reflected energy level for these receivers was averaged to provide a single number value for each height of receiver plane per octave band per room. This provides an indication of how strong the retroreflection is around the source location. For the near-field and far-field analysis, a linear regression was calculated, from which spatial decay rates (in decibels per unit distance) were derived for each field per room per octave band. This provides an indication of how tight the focus is.

4 RESULTS AND DISCUSSION

All simulations performed show a greater amount of retroreflected sound energy at higher frequencies compared to a flat ceiling. Also, low frequencies show a rise in reflected sound energy where the retroreflector array corner cube size was increased. Figure 2 shows the summed retroreflected energy per octave band in each room, where the 0.3 m array room reveals greater reflected energy at higher frequencies, providing approximately 4 dB of reflected energy at 8 kHz at 1 m away from the retroreflective surface, whereas a flat specular surface yields -4 dB at 8 kHz for a 1 m height. Similarly, the 0.6 m array room provides an elevated response for mid frequency bands, showing about 4 dB of reflected energy at 1 kHz, compared to -4 dB at 1 kHz for the specular flat ceiling room. From the 0.9 m and 1.2 m array rooms, a flatter response can be noticed for all the heights, as the size of the elements increases. Figure 2 also shows that the retroreflected energy tends to decrease with increasing height for each room, but less so for the larger array element sizes.

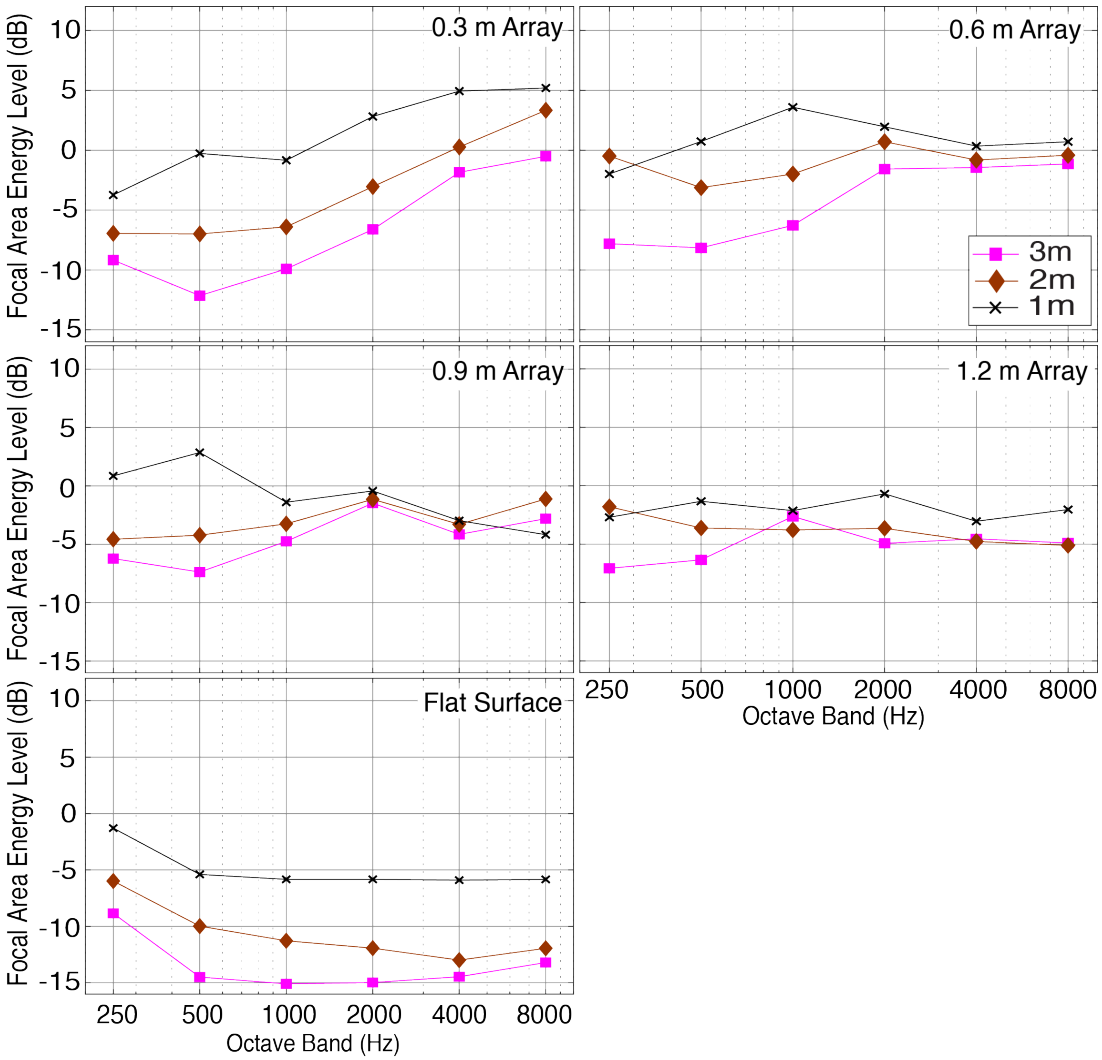

Figure 2: Retroreflected energy for each room within the focal area (0m – 0.15 m) for each source and receiver array height relative the direct sound energy at 1 m, in octave bands.

The contrast between the corner cube array cases and the specular case increases with distance. However, the larger corner cube arrays yield more consistent results with distance.

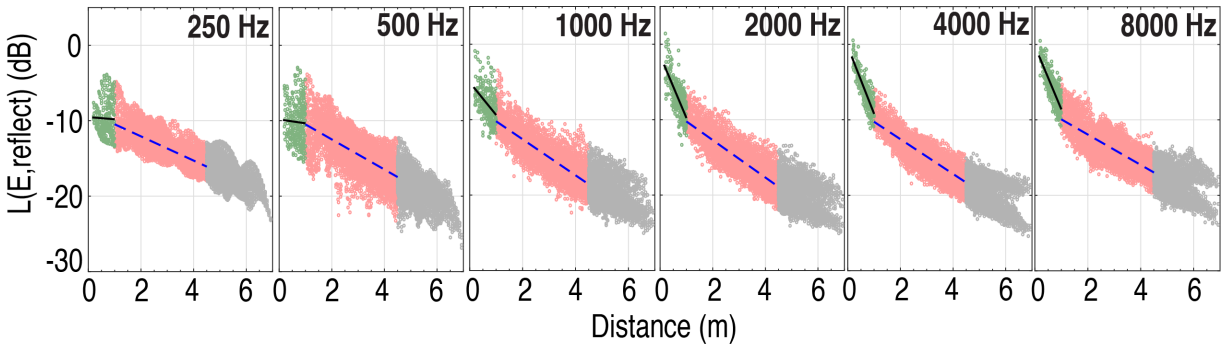

Figure 3: Reflected energy for all receivers in the 0.6 m room at a height of 3 m per octave band relative to the direct sound at 1 m, with linear regression lines for Near-field (black line, green scatter points), Far-field (blue dashed line, pink scatter points) and remaining scatter points (grey)

The spatial decay rates of the various rooms are shown in figure 4, in which the retroreflective effect is also apparent. The bottom axis of the figure refers to the height of the source-receiver plane, followed by either the near field (N, 306 receivers) or the far field (F, 6038 receivers) indicator. Significance of the linear regressions were consistently strong (p<0.0001) (fig. 3). The near field spatial decay rate is often higher than the far field rate when the surface is acting as a retroreflector. For the 4 kHz and 8 kHz bands, the near field values for the 0.3 m and 0.6 m array rooms show a higher decay rate, ranging from about 7 to 10 dB/m at all heights. However, the largest array (1.2 m) does not achieve as high spatial decay rates in any of the conditions tested.

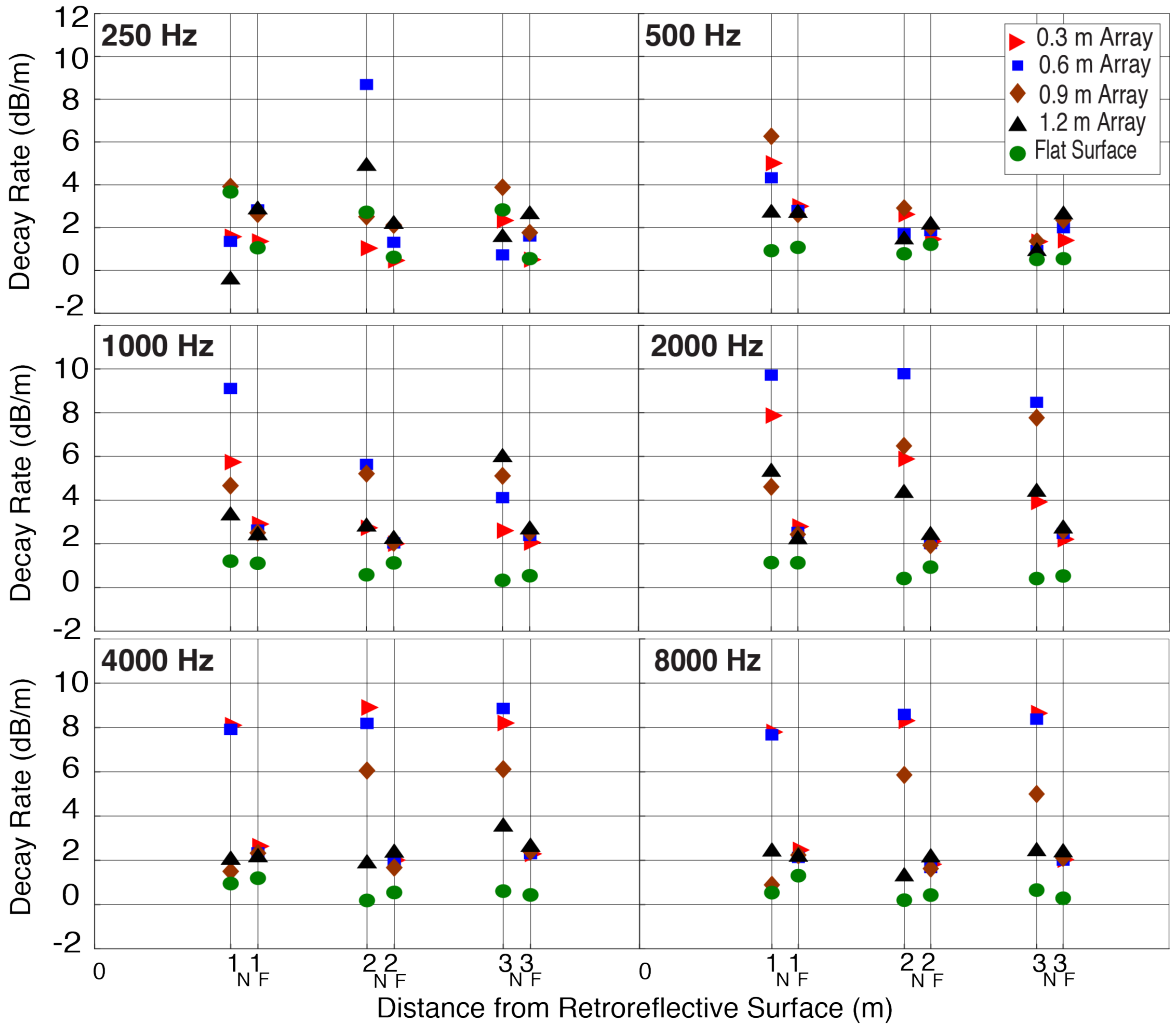

Figure 4: Octave band spatial decay rates of reflected energy, derived from linear regression as a function of distance relative to the direct sound energy at 1 m. The three separate heights are expressed (e.g., 1N or 1F) relates to either Near field analysis ('…'N = 0.15 m to 1 m) of Far field analysis ('…'F = 1 m to 4.5 m) and their individual height (1 m – 3 m).

The lower frequency bands show only a small decay over the near and far field, presumably due to long wavelengths relative to the retroreflective elements. The 0.6 m array room provided an outlying decay rate at 250 Hz for the 2 m height, the cause of which is not clear. Interestingly, the 1 kHz and 2 kHz band charts show that the 0.6 m room provides an increased decay rate at 1 kHz at the 1 m height in the near field, while showing an almost steady decay rate between 8 to 10 dB for all heights in the near field at 2 kHz. Far field decay rates are mostly not much greater than for the specular case.

Finally, a clear distinction can be made between the specular ceiling room and retroreflective ceiling rooms, where the reflected energy for the specular room does not vary much between octave bands or different heights. This

highlights the effectiveness of retroreflectors in terms of reflecting energy to a focal point (at the source) compared to a commonplace flat surface, and shows that there is often rapid decay with distance from this focus (mainly near field), depending on the corner cube size and ceiling height.
Figure 5 shows the reflected energy levels for all receivers for each receiver plane height (1 – 3 m) for the 0.6 m corner cube array. The figure shows that with increasing distance, the focal area retains sound energy, whilst the receivers in the far field yield a steeper decay.

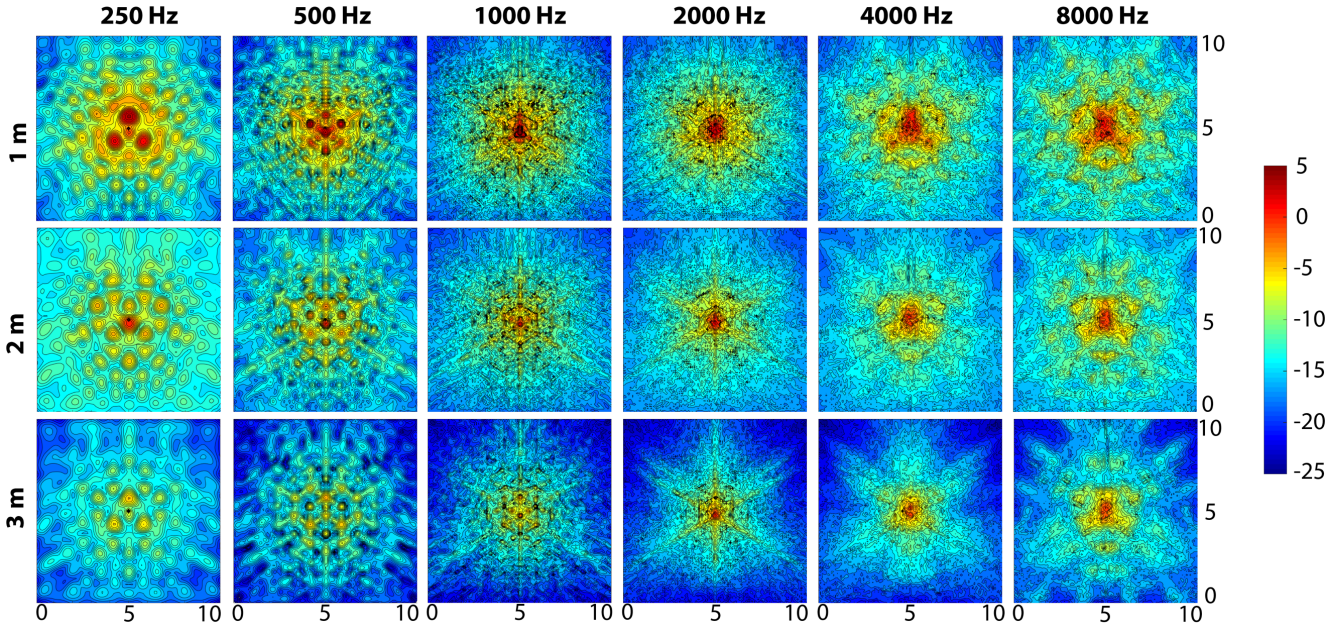

Figure 5: Reflected energy levels for the 1 m, 2 m and 3 m receiver plane height, per octave band and relative to the direct sound at 1 m for the 0.6 m corner cube array.

Drawing on these results, if we consider the example of a 0.6 m corner cube array, it appears to have particular potential in providing voice support to people talking (i.e., returning the energy of each person's voice back to them for moderate ceiling heights). With a ceiling either 2 or 3 m above centre-of-head, this surface consistently provides both strong reflected energy in the focus in the mid- and high-frequency range (fig. 2), and a rapid spatial decay in the near field (fig. 3,4). However, a limitation of this work is that the source and receivers were omnidirectional – further study is required to examine how speech directivity affects the effectiveness of various acoustic retroreflector array configurations.

5 CONCLUSION

Although acoustic retroreflection in architecture is still a scarcely used concept, this study highlights its potential to provide increased reflected energy at and around sound sources and a steep spatial decay rate within the source's near field. These results especially show that retroreflection from corner cube arrays of the dimensions studied can be highly effective for the spectrum bands important for speech. Hence we hypothesise that a retroreflective surface could focus its reflections back onto a talker (or onto multiple individual talkers), potentially introducing a reverse Lombard effect (Lau, 2008) influencing the talker(s) to lower their voice. One of the next steps in this study will include an application of retroreflective surfaces to the open-plan office issue of speech distraction, and the general effect of different types of retroreflective surfaces within multi-talker environments.

ACKNOWLEDGEMENTS

The authors thank Jonothan Holmes for his continuous support and insight, and acknowledge the facilities, and the scientific and technical assistance of the Sydney Informatics Hub at the University of Sydney and, in particular, access to the high performance computing facility Artemis. This work was done as part of a research project

entitled *Robotic Design and Fabrication of Spatial Structures and Integrated, Acoustically Effective, Responsive Ceiling System for A Workspace Environment*, led by Dagmar Reinhardt (University of Sydney) and Ninotschka Titchkosky/Matthew Blair (BVN Architecture Pty Ltd).

REFERENCES

Bilbao, Stefan. 2013. 'Modeling of Complex Geometries and Boundary Conditions in Finite Difference/Finite Volume Time Domain Room Acoustics Simulation'. IEEE Transactions on Audio, Speech, and Language Processing 21 (7): 1524–33. https://doi.org/10.1109/TASL.2013.2256897

Cabrera, Densil, Jonothan Holmes, Hugo Caldwell, Manuj Yadav, and Kai Gao. 2018. 'An Unusual Instance of Acoustic Retroreflection in Architecture – Ports 1961 Shanghai Flagship Store Façade'. Applied Acoustics 138 (September): 133–46. https://doi.org/10.1016/j.apacoust.2018.04.004.

Cox, Trevor J. and Peter D'Antonio. 2009, 'Acoustic Absorbers and Diffusers: Theory, Design and Application.' London: Spon Press. 495

Crawford, Frank S. 1991. 'Cube Corner Retroreflectors for Sound Waves'. American Journal of Physics 59 (2): 176–77. https://doi.org/10.1119/1.16601.

Van Duyne, Scott A., and Julius O. Smith. "Physical modeling with the 2-D digital waveguide mesh." In Proceedings of the International Computer Music Conference, pp. 40-40. INTERNATIONAL COMPUTER MUSIC ACCOCIATION, 1993.

Haapaniemi, A. 2012. "Simulation of acoustic wall reflections using the finite difference time-domain method." PhD diss., Master's thesis, Aalto University, Finland,

Hannouch, A. Caldwell, H. Cabrera, D. and Reinhardt, D. 2018 and published by the Association for Computer-Aided Architectural Design Research in Asia (CAADRIA) in Hong Kong: T. Fukuda, W. Huang, P. Janssen, K. Crolla, S. Alhadidi (eds.), Learning, Adapting and Prototyping, Proceedings of the 23rd International Conference of the Association for Computer-Aided Architectural Design Research in Asia (CAADRIA) 2018, Volume 1, 317-325.

Kowalczyk, K. 2008. 'Boundary and medium modelling using compact finite difference schemes in simulation of room acoustics for audio and architectural design applications.' PhD thesis, School of Electronics, Electrical Engineering and Computer Science, Queen's University Belfast.

Kowalczyk, Konrad, and Maarten van Walstijn. 2011. 'Room Acoustics Simulation Using 3-D Compact Explicit FDTD Schemes'. IEEE Transactions on Audio, Speech, and Language Processing 19 (1): 34–46. https://doi.org/10.1109/TASL.2010.2045179.

Lau, Priscilla. 2008. "The Lombard Effect as a communicative phenomenon." UC Berkeley Phonology Lab Annual Reports 4, no. 4.

Lombard, E. 1911. Le signe de l'elevation de la voix. Annales des Maladies de l'Oreille, du Larynx, du Nez et du Pharynx, 37, 101-119

Saarelma, Jukka. 2013. "Finite-difference time-domain solver for room acoustics using graphics processing units." Master's thesis, Aalto University, Finland.

Schneider, John B, Christopher L Wagner, and Omar M Ramahi. 1998. 'Implementation of Transparent Sources in FDTD Simulations'. IEEE TRANSACTIONS ON ANTENNAS AND PROPAGATION 46 (8): 10.

Smith, Julius O. 1992. 'Physical Modeling Using Digital Waveguides'. Computer Music Journal 16 (4): 74. https://doi.org/10.2307/3680470.

Van Duyne, Scott A., and Julius O. Smith. 1995. "The tetrahedral digital waveguide mesh." In Applications of Signal Processing to Audio and Acoustics, 1995., IEEE ASSP Workshop on, pp. 234-237. IEEE.

Yee, K. S. "Numerical solution of initial boundary value problems involving Maxwell's equations in isotropic media." IEEE Trans. Antennas Propagation 14, no. 5 (1966): 1327-1333.